Vitrification is a spontaneous non-equilibrium transition driven by osmotic pressure

J. Galen Wang and Roseanna N. Zia*

Department of Chemical Engineering, Stanford University, Stanford, CA 94305

February 28, 2021

Abstract

Persistent dynamics in colloidal glasses suggest the existence of a non-equilibrium driving force for structural relaxation during glassy aging. But the implicit assumption in the literature that colloidal glasses form within the metastable state bypasses the search for a driving force for vitrification and glassy aging and its connection with a metastable state. The natural relation of osmotic pressure to number-density gradients motivates us to investigate the osmotic pressure as this driving force. We use dynamic simulation to quench a polydipserse hard-sphere colloidal liquid into the putative glass region while monitoring structural relaxation and osmotic pressure. Following quenches to various depths in volume fraction ϕ (where $\phi_{RCP} \approx 0.678$ for 7% polydispersity), the osmotic pressure overshoots its metastable value, then decreases with age toward the metastable pressure, driving redistribution of coordination number and interparticle voids that smooths structural heterogeneity with age. For quenches to $0.56 \leq \phi \leq 0.58$, accessible post-quench volume redistributes with age, allowing the glass to relax into a strong supercooled liquid and easily reach a metastable state. At higher volume fractions, $0.59 \leq \phi < 0.64$, this redistribution encounters a barrier that is subsequently overcome by osmotic pressure, allowing the system to relax toward the metastable state. But for $\phi \geq 0.64$, the overshoot is small compared to the high metastable pressure; redistribution of volume stops as particles acquire contacts and get stuck, freezing the system far from the metastable state. Overall, the osmotic pressure drives structural rearrangements responsible for both vitrification and glassy age-relaxation. We leverage the connection of osmotic pressure to energy density to put forth the mechanistic view that relaxation of structural heterogeneity in colloidal glasses occurs via individual particle motion driven by osmotic pressure, and is a spontaneous energy minimization process that drives the glass off and back to the metastable state. This connection of energy, pressure, and structure identify the glass transition, $0.63 < \phi_g \leq 0.64$.

*rzia@stanford.edu

1 Introduction

Molecular theories have been successfully adapted to predict phase separation and crystallization in colloidal dispersions and other complex fluids, resulting in powerful tools for engineering industrial materials. However, sometimes the liquid-to-solid transition in colloids occurs without crystallization, leading to formation of a solid with amorphous structure — a colloidal glass. The ability to model and predict the colloidal glass transition is a broadly impactful problem both scientifically and industrially: vitrification plays a role in bacterial fitness and other biological soft matter [1–4], geophysical dynamics, and is central to industrial coatings [5–7], food processing [8, 9], and materials engineering. Unlike molecular materials, both crystallization and vitrification can be induced in colloids simply by changing particle concentration [10]. But as with molecular glasses, attempts to adapt equilibrium theories to describe and predict the colloidal glass transition have met with limited success, because equilibrium models — typically utilizing free-energy minimization approaches — fail to predict a glassy state; instead, they predict that there is always a crystalline state at the lowest free energy for volume fractions $\phi > 0.494$, for both monodispserse [11] and polydisperse colloidal systems up to 14% polydispersity [12–14]. These findings support the now widely-accepted idea that glasses do not form in thermodynamic equilibrium and the glassy 'state' cannot be located via an equilibrium free-energy minimization arguments.

More successful models assume that the glass is in a metastable equilibrium state by way of being an extrapolation of the equilibrium liquid state. The most prominent of these include Mode-Coupling Theory (MCT) [15, 16], Random First Order Transition Theory (RFOT) [17–19] and Activated Barrier Hopping Theory (ABHT) [20–23]. The assumption of metastable equilibrium permits such approaches to adapt equilibrium liquid theories to the colloidal glass transition. For example, both MCT and ABHT employ a dense form of the Percus-Yevick closure for the radial distribution function (which is formally correct only for the liquid) with no change in the partition function. A discussion of these theories can be found in [24], among others. The glassy phase can thus appear as a metastable line that ostensibly can be followed via a presumably infinitely slow quench, where equilibrium is achieved upon each sequentially small increase in volume fraction. The problem with the idea of glass formation in a metastable state becomes clear when one attempts to describe how a system achieves and remains 'arrested' in the metastable state without falling to the lower free-energy crystalline state: a monodisperse set of colloids easily crystallizes, falling nearly instantaneously off the metastable line to the underlying crystalline state. Weak polydispersity delays this fall but permits eventual crystallization, offering some hope for the idea of metastability. But for a colloidal system at polydispersity between 7% and 14%, where crystallization is theoretically possible, quenches into the solid region do not permit crystallization or even a metastable state, over observable time scales. Overall, we suspect that the metastable state itself may be an underlying or fictitious state, because in practice the metastable line is difficult to construct: a system will either near-instantaneously fall down to the crystalline state due to thermal fluctuations, or get pushed off the metastable line onto a non-equilibrium glassy branch.

The difficulty of achieving the metastable line evinces a qualitative shift in dynamics, for which

we have already found evidence in our prior work: a qualitative change of particle dynamics in quenches deeper than the liquid [24]. This leads to our primary objection to the use of equilibrium liquid-state dynamics in glass theories to predict the behavior of the solid state. The use of the assumption that liquid dynamics are qualitatively the same as glassy dynamics — along with the *ad hoc* enforcement of divergent extrapolation of dynamics from the liquid state to the solid state — are directly linked to very wide variations in the prediction of the volume fraction at which putatively divergent relaxation time emerges. An equally serious consequence is that the implicit assumption typically invoked, that colloidal glasses form within the metastable state, effectively bypasses the search for a driving force for vitrification and glassy aging, much less its connection to the long-time metastable state. Indeed, these equilibrium approaches fail to identify a driving force that could give a path to the crystallization they themselves hypothesize exists.

But the fact that some glasses give way to crystals with time [25, 26] suggests that aging is a key behavior that must be captured in models of vitrification. In fact, it has been thoroughly demonstrated in experiments that molecular glass-formers age to a lower energy state following any quench that is not infinitely slow [27, 28], suggesting that some force pushes the system off the metastable "supercooled" liquid line. Only after this occurs can the system age toward the metastable state. This behavior evinces the hindered ability of the system particles to diffuse into an equilibrium arrangement before getting locked into position, similar to the role played by size polydispersity and fast quenches in colloidal glasses. As with molecular glasses, colloidal glasses age with time. But few glass theories address aging [29, 30] or explicitly study the impact of the actual quench, which takes time. Instead, numerical approaches form glassy configurations via event-driven energy minimization algorithms, without Brownian dynamics. The few studies that report the effect of quench rate in colloidal glasses conclude that long-time structure as well as the glass transition volume fraction ϕ_g is independent of the quench rate [31, 32]. Subsequent studies identified that the quench-rate dependence of glass properties is more relevant in soft colloids [33], but the effects of quench rate on the dynamics of vitrification or crystallization are not discussed. Overall, post-quench aging suggests that colloidal glasses are spontaneously driven off some metastable path; this mechanism could also drive structural age-evolution toward the metastable state. Understanding the interplay between quench rate and particle dynamics could thus be valuable for developing predictive theory, which is why in the present work we form colloidal glasses interrogating this behavior by explicitly quenching from the liquid into the solid region.

We showed in our prior work that, after a quench from the liquid into the colloidal glass [24], aging is a process during which the system relaxes via long-time but short-range self-diffusion ("dense diffusion") toward an intransient state, as the system explores many configurations. Relaxation time remains finite – it does not diverge, even deep into the glass, reinforcing the need for a more complete mechanistic model of vitrification. It is reasonable to infer that the evolution to an intransient state is a process that smooths local concentration gradients. The idea that number-density gradients in osmotic pressure drive diffusive colloidal migration was first put forth by Einstein in his theory of Brownian motion [34]. Temporary number-density gradients arise from the separation between the time scale of colloidal inertial relaxation and the solvent time

scale. The Brownian relaxation time scale determines how quickly these gradients are smoothed by Brownian diffusion, and the denser the suspension, the slower the relaxation. The connection between osmotic pressure and number-density fluctuations has since been successfully expanded to semi-dilute-to-moderately-concentrated colloids and flowing colloidal suspensions [35–39], which inspired us to hypothesize that a similar process takes place in colloidal glasses involving volume fraction quenches: as the heterogeneous void density forms during the concentration quench, osmotic pressure accumulates and pushes the system out of equilibrium and remains "arrested" there. This accumulated or non-equilibrium osmotic pressure subsequently provides a driving force for a minimization process back towards the metastable equilibrium state through age relaxation. The connection between osmotic pressure and energy density suggests the possibility of a spontaneous process of energy minimization. We test our hypotheses utilizing dynamic simulations to access the particle-scale detail of coordination number, local number density and void space, and particle-phase osmotic pressure, quantities that are challenging to measure in experiments.

The remainder of this paper is organized as follows: In §2 we present the model system as well as our simulation method. Results are presented in §3, divided into two parts. In the first, we examine structural evolution. In the second, we report the evolution of osmotic pressure following the quench. The study is concluded with a discussion in §4.

2 Methodology

2.1 Model system

We consider a colloidal suspension composed of 55,000 neutrally buoyant, hard colloidal spheres of radius a and density ρ_p suspended in a Newtonian solvent of density ρ and viscosity η. Fluid motion is governed by the Stokes equations owing to a vanishingly small Reynolds number and Stokes number associated with the small size of colloids, $Re = \rho U a/\eta \ll 1$ and $St = \rho_p/\rho Re \ll 1$. Here, U is the characteristic particle velocity set by Brownian diffusion. The colloid volume fraction is defined as $\phi = 4/3n\pi\eta a^3$, where n is the particle number density. The initial volume fraction of the system is $\phi = 0.35$, which is subsequently quenched to final values in the range $0.40 \leq \phi = 0.68$, spanning the liquid to the highly concentrated glassy state. Particle-size polydispersity $s = 7\%$ is implemented to represent experimental systems that do not readily crystallize. The particles interact via an interparticle potential $V(r)$. The purpose of this work is to study the most fundamental aspects of the colloidal glass transition, the entropic exclusion and Brownian motion that determine phase behavior. To that end, we utilize a strongly repulsive, short-range Morse potential:

$$V(r) = -V_0 \left(2\mathrm{e}^{-\kappa[r-(a_i+a_j)]} - \mathrm{e}^{-2\kappa[r-(a_i+a_j)]}\right), \tag{1}$$

which describes a nearly-hard sphere interaction between particles i and j separated by a distance r. Here V_0 indicates the minimum of the potential and κ^{-1} represents the "width" of the potential well. The combination of these two parameters control how hard the particles are; the larger V_0 and κ, the harder the particles. We choose $V_0 = 6kT$ and $\kappa = 30/a$; these parameters, together

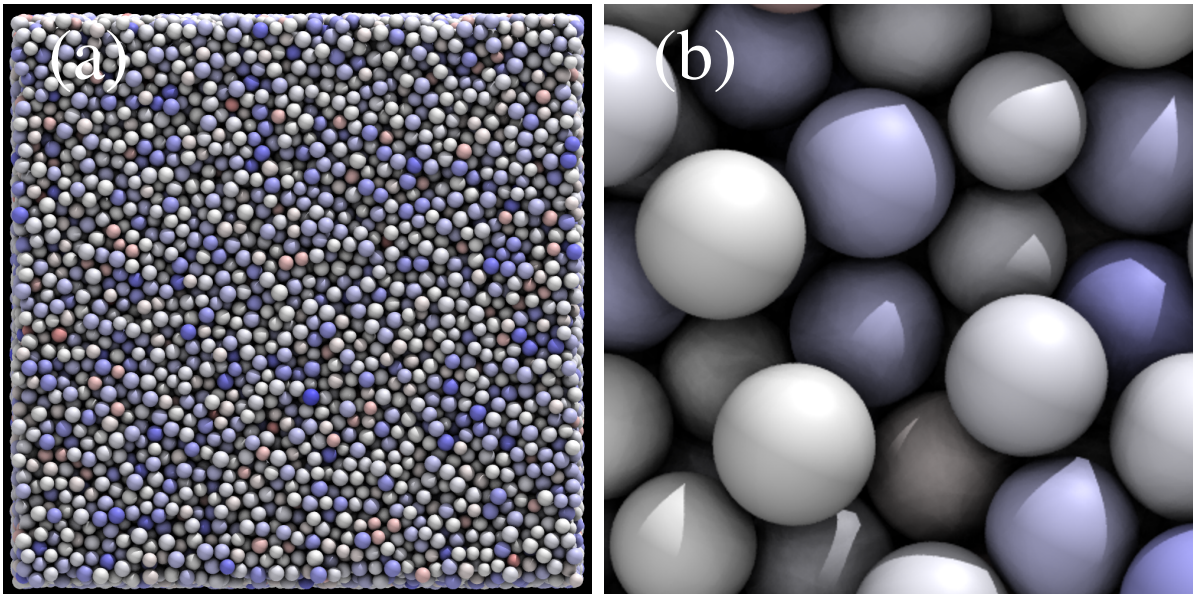

Figure 1: Simulation model system. (a) Snapshot of one periodic simulation cell at the final volume fraction $\phi_{final} = 0.63$. The color indicates the number of contacts of each particle; the color changes from red to white to blue as the number of contacts varies from 0 to 12. (b) 10x magnification. From [24], with permission.

with the exponential nature of the Morse potential, give a good approximation to hard spheres [40]. We set a cutoff distance at exactly the minimum of the potential to model a purely repulsive system. Each particle experiences hydrodynamic drag and undergoes Brownian motion; many-body hydrodynamic interactions are neglected.

2.2 Dynamic simulation method

We conduct Brownian Dynamics simulations utilizing the LAMMPS molecular dynamics package [41] which provides an ideal platform due to its parallelization scheme that is highly optimized to handle large particle systems. 55,000 Brownian particles are randomly distributed throughout the simulation box, which is periodically replicated to model an infinite system. To suppress crystallization, we implemented 7% size polydispersity, the lowest value of polydispersity shown to prevent crystallization [13, 14, 42, 43]. We assign each particle to one of five evenly distributed sizes $0.9a$, $0.95a$, $1.0a$, $1.05a$, $1.1a$, with each size group containing one-fifth of the total number of particles. Measurements of particle separation take into account this size distribution. To confirm that 7% size polydispersity is sufficient to suppress crystallization, we monitored the crystal fraction throughout the system by measuring the 6-point local order parameter q_6 [44]. We found that the crystal fraction remains less than 0.01% (less than 0.01% of particles have a local order of $q_6 > 0.3$) throughout the simulation. Figure 1 shows a rendered image of one simulation cell and a zoomed-in snapshot, showing the crowded structure of a colloidal glass at $\phi = 0.63$.

Colloidal particles interact via hydrodynamic $\boldsymbol{F}^H$, Brownian $\boldsymbol{F}^B$, and interparticle $\boldsymbol{F}^P$ forces, which subsequently produce motion governed by the Langevin equation, a stochastic force balance

on each particle:

$$\boldsymbol{m} \cdot \frac{d\boldsymbol{U}}{dt} = \boldsymbol{F}^H + \boldsymbol{F}^B + \boldsymbol{F}^P. \tag{2}$$

Hydrodynamic interactions play a role in suspension mechanics even up to (and likely beyond) volume fractions as high as 55%. But when the repulsion range between particles keeps their no-slip surfaces separated by at least twenty percent of their size, these interactions become quite weak. The study of such freely-draining suspensions is often essential to gleaning fundamental insights about entropic forces and has led to many landmark discoveries [45–48] We take the freely-draining approach in the present study and thus make the simplifying assumption that the hydrodynamic force on each particle is determined by Stokes' drag law:

$$\boldsymbol{F}_i^H = -6\pi\eta a_i \left[\boldsymbol{U}_i - \boldsymbol{u}^\infty(\boldsymbol{X}_i)\right]. \tag{3}$$

Here, $\boldsymbol{U}_i - \boldsymbol{u}^\infty(\boldsymbol{X}_i)$ represents the particle velocity $\boldsymbol{U}_i$ relative to the fluid velocity $\boldsymbol{u}^\infty(\boldsymbol{X}_i)$. In this work, there is no imposed flow, $u^\infty(X_i) = 0$, in order to avoid structural bias induced by flow that could seed crystallization or otherwise alter the glass transition. The Brownian force obeys Gaussian statistics [49]:

$$\overline{\boldsymbol{F}_i^B} = 0,\ \overline{\boldsymbol{F}_i^B(0)\boldsymbol{F}_i^B(t)} = 2kT(6\pi\eta a_i)\boldsymbol{I}\delta(t), \tag{4}$$

where the overbars indicate averaging over a time period larger than the solvent timescale and $\mathbf{I}$ is the identity tensor. The Dirac delta distribution $\delta(t)$ indicates that the Brownian impacts are instantaneously correlated. The interparticle force is defined as the negative gradient of the interparticle potential $V(r)$, and because the Morse potential is spherically symmetric, we incorporate its derivative in the spherical coordinate system:

$$\boldsymbol{F}_i^P = -\sum_j \frac{\partial V(r_{ij})}{\partial r_{ij}} \hat{\boldsymbol{r}}_{ij}. \tag{5}$$

Here, $\boldsymbol{r}_{ij} = \boldsymbol{r}_{ij}/r_{ij}$, where $\boldsymbol{r}_{ij} = \boldsymbol{X}_i - \boldsymbol{X}_j$ is the separation vector from the center of particle i to the center of particle j, and $r_{ij} = |\boldsymbol{r}_{ij}|$. The summation is over all the interacting pairs involving particle i. In LAMMPS, particle velocities and positions are advanced in time numerically using Verlet integration [50]. To faithfully model colloidal physics, both the Reynolds number and the Stokes number must be small; in LAMMPS, this requires careful selection of the integration time step, which we set to be $\Delta t = 10^{-6}a^2/D$, where a^2/D is the diffusive time required for a single particle of size a diffusing its size in a pure solvent with diffusion coefficient $D = kT/6\pi\eta a$. The small time step permits only very small particle overlaps, which is resolved via a standard Heyes-Melrose algorithm [51]. This overlap resolution represents an entropic encounter that contributes appropriately to the osmotic pressure[38, 40].

Our simulation of colloidal glass comprises two physical processes. First, the system is "quenched" from the moderate-volume fraction liquid state to a high-volume fraction solid state. We effect the glass transition using an algorithm we previously developed [24], in which we rapidly increase

the size of each particle at fixed system volume, thus effecting a volume fraction jump. In this study, we fix the initial volume fraction $\phi_{initial} = 0.50$, which is a liquid state for our polydisperse system [13, 14, 52]. We vary the final volume fraction in the range $0.56 \leq \phi_{final} \leq 0.68$, which spans the supercooled liquid to the putative glass transition ($\phi = 0.58$) to the jamming transition at $\phi = 0.68$ [53]. Choosing the initial liquid state as close as possible to the glassy state mitigates the effect of "τ-effective paradox" [27], which describes the undesirable history dependence of material's equilibrium mobility. We execute a fast quench rate $d\phi/dt = 0.25D/a^2$, which permits the volume fraction quenches to take place between $0.04 \leq t/(a^2/D) \leq 0.72$ so that the structure does not have time to relax during the quench, freezing in liquid structure. Overall, our particle-size jump method minimizes the bias from external shear that is often employed in experiments. The second process modeled in our simulations is aging. After the final volume fraction is reached, we hold the system at an iso-volume-fraction condition, letting it evolve under the action of Brownian motion, hard-sphere repulsion, and Stokes drag, allowing it to age to $t/(a^2/D) = 20,000$.

During and following each jump, the positions, velocities, and particle-phase stress are tracked and utilized to characterize age relaxation. We quantify the detailed particle structure by measuring the particle coordination number, which is defined as the number of particles with surface-to-surface separation of $0.05a$ from a reference particle. Because particles undergo Brownian motion, the first shell of nearest neighbors around a particle are not located precisely at $r = 2a$, which would lead to a sharp peak in the structure. Instead, they fluctuate about $r = 2a$, which gives the familiar, slightly broader peak. Conventional structural measurements like the static structure factor or radial distribution function require averaging over the entire domain, which obscures localized variations. Instead, we monitor the detailed positions for all particles throughout the simulation and, from it, infer the temporal evolution of coordination number and heterogeneous free volume throughout the glass.

To explore the relationship between osmotic pressure and structural relaxation, we monitor the particle-phase stress $\mathbf{\Sigma}^P$, above and beyond the fluid stress and, from it, compute the particle-phase osmotic pressure averaged over the entire suspension. The particle-phase stress $\mathbf{\Sigma}^P$ in a freely-draining suspension arises from the ideal osmotic pressure $nkT\mathbf{I}$ and the interparticle elastic stress $\boldsymbol{r}\boldsymbol{F}^P$:

$$\langle \mathbf{\Sigma} \rangle = -nkT\boldsymbol{I} - n\left\langle \boldsymbol{r}\boldsymbol{F}^P \right\rangle, \tag{6}$$

where the angle brackets indicate an average over all particles. The particle-phase osmotic pressure is defined as negative one third of the trace of particle-phase stress $\mathbf{\Sigma}^P$:

$$\langle \Pi^P \rangle = -\frac{1}{3}\boldsymbol{I} : \langle \mathbf{\Sigma}^P \rangle. \tag{7}$$

The osmotic pressure, with units of energy per unit volume, is closely related to the free energy, which has both an energy term and an entropy term. In our freely-draining model, the osmotic pressure only depends on the interparticle stress $\mathbf{\Sigma}^P = \langle \boldsymbol{r}\boldsymbol{F}^P \rangle$, where $\boldsymbol{r}$ is the vector connecting the centers of an interacting pair of particles and $\boldsymbol{F}^P$ is the interparticle force which is derived from the interparticle potential (Equation 5). This can be an attractive potential as in the case

of gels, or it can be a repulsive potential that is steep or soft, short- or long-ranged. Indeed, other mechanisms such as particle deformability influence the location of the glass transition and the relaxation spectrum available to the material [54–58], and the contribution of these mechanisms are included in osmotic pressure. Thus, the average potential energy of the system $\langle V \rangle$ is determined given the particle configuration, which comes from a configurational space that is related to the entropy S. The free energy $\langle F \rangle$ can then be written as $\langle F \rangle = \langle V \rangle - TS$ [59]. We propose that osmotic pressure acts to minimize this free energy in a glass, which it does by smoothing the local concentration gradient, acting to reduce the average potential energy and increase the entropy.

3 Results

We have hypothesized that the heterogeneous number-density gradients in newly-formed colloidal glasses give rise to osmotic pressure gradients that drive structural relaxation toward a metastable state that has homogeneous particle distribution. In this section we present our results that connect measurements of particle distribution, mesoscale structure, and osmotic pressure to a mechanistic explanation for vitrification. In order to investigate the idea that heterogeneous cages form and relax during vitrification, we monitor structural relaxation via two measurements: coordination number and void distribution. This is followed by a study of the osmotic pressure as it evolves with age. We start our simulations of hard-sphere colloids with in the liquid state, $\phi = 0.50$ with 7% polydispersity, and quench rapidly into more concentrated states near and into the putative glass, with a final volume fraction ranging from $0.56 \leq \phi \leq 0.68$ (recalling that with 7.5% polydispersity, random-close packing occurs at $\phi_{rcp} \approx 0.676$ [53]). We then monitor particle positions and osmotic pressure as the glass ages over time. We remark that our particle-size quench model represents a physical process that mimics experiments to generate a non-equilibrium configuration, and we emphasize that a fast "quench" is necessary to form a glass; otherwise a crystalline state will form. Thus, the post-quench aging behavior reveals a spontaneous mechanism that drives the colloidal glass transition.

3.1 Structural relaxation

To get a sense of how quench depth affects the post-quench structural evolution of a colloidal glass, we examine the coordination-number distribution, $P(N_c)$, which gives one measure of how caged each particle is. The number of particles with a given coordination number N_c gives a distribution $P(N_c)$ that offers additional information beyond the pair-distribution function (PDF). The PDF emerges from (but smears out) a tabulation of the distribution of distances between particle pairs, giving an average cage size around a reference particle, as well as for larger and larger surrounding cages, but cannot give information about heterogeneity. In Figure 2, we plot the evolution of the coordination number distribution $P(N_c)$ for several values of final volume fraction. Going from panel (a) to (b) to (c) to (d), the long-time peak coordination number moves monotonically to the right with increasing quench depth. However, the wait-time evolution of $P(N_c)$ gives a

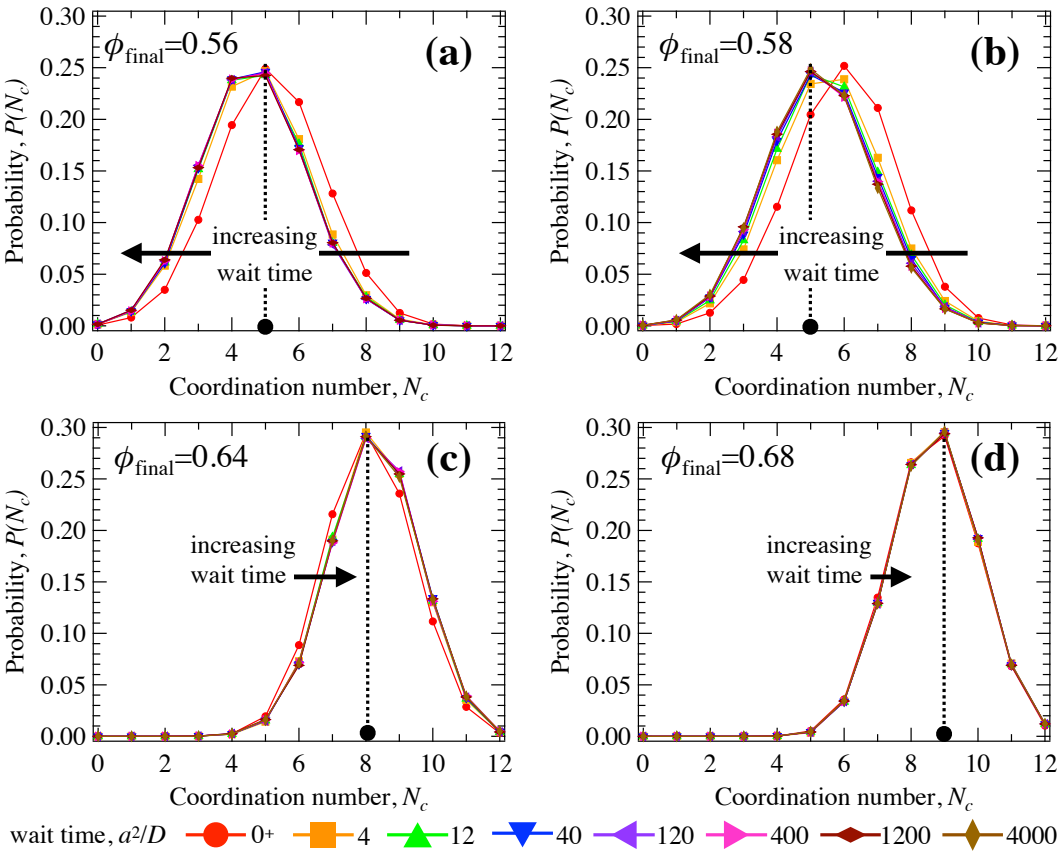

Figure 2: Evolution of coordination number distribution as a function of wait time, at volume fractions (a) $\phi = 0.56$, (b) $\phi = 0.58$, (c) $\phi = 0.64$, and (d) $\phi = 0.68$. The arrow in each panel indicates the direction (increase or decrease) toward which the contact number evolves. The dashed lines indicate the peak location of the coordination number distribution at the longest wait time ($4,000a^2/D$).

surprising result: it is non-monotonic in volume fraction. For $0.56 \leq \phi \leq 0.58$, $P(N_c)$ relaxes to lower values with wait time, with the most significant change shortly post quench, followed by less obvious change thereafter. This relaxation to fewer neighbors for all particles suggests quenching just into the glassy region produces a structure with appreciable interstitial free volume that is heterogeneous immediately post quench, which then produces a strong initial driving force to relax the system to a less frustrated state. However, this trend reverses for $\phi \geq 0.64$, where N_c shifts toward larger values. The amount of the shift decreases with volume fraction, which reflects the physically intuitive result that there is much less interstitial free volume deep into the glass. As a result, the driving force to redistribute volume is frustrated: the nearest-neighbor cages become so tight that steric hindrance prevents particles from further relaxation. The change in the distribution of coordination numbers shows that structural heterogeneity manifested in the abundance of "looser" cages (lower coordination number) and "tighter" cages (higher coordination number) get redistributed, presumably to produce a more homogeneous structure. To get an idea of how relaxation homogenizes the structure for each coordination number group, we interrogate the average coordination number, which tells us how, on average, the amount of caging has changed.

The coordination number is monitored throughout simulation and we compute its average over

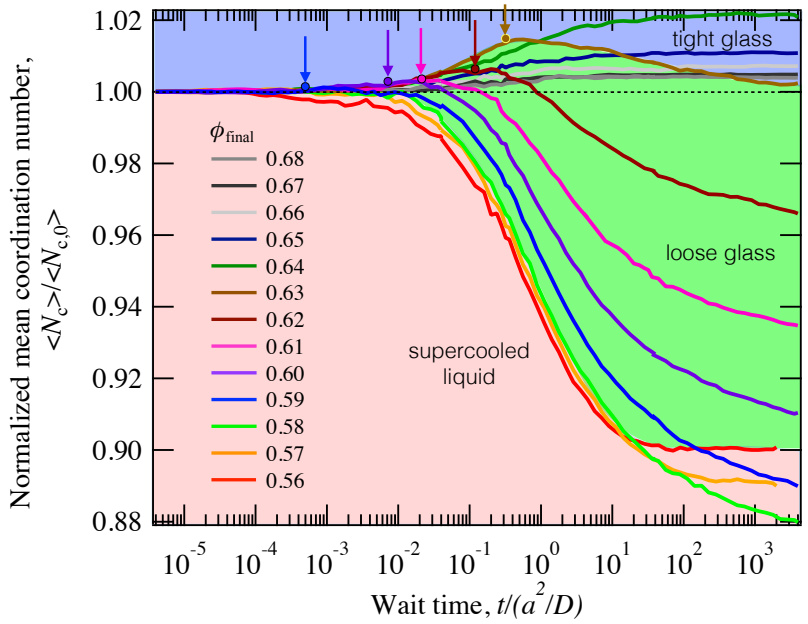

Figure 3: Evolution of mean coordination number normalized by the value just after the jump as a function of wait time. Based on different behavior of mean coordination number, the figure is shaded into red ($\langle N_c \rangle$ decreases with wait time then plateaus), green ($\langle N_c \rangle$ increases then decreases) and blue ($\langle N_c \rangle$ increases with wait time then plateaus) regions. The downward arrows indicate the peak location of normalized $\langle N_c \rangle$ for those loose glass at $0.58 < \phi < 0.64$.

all particles for all quench depths studied. We normalize it on its initial value $N_{c,0}$ immediately following the quench, and plot this quantity, $\langle N_c \rangle / \langle N_{c,0} \rangle$ as a function of wait time (age) in Figure 3. For volume fractions below 58%, there is a monotonic decrease in the average coordination number over time, suggesting that the post-quench cages are loose enough to easily permit relaxation. Interestingly, at long times, a deeper quench results in a more complete relaxation, suggesting that structural heterogeneity provides a driving force for relaxation, with stronger heterogeneity providing a stronger driving force. We identify these glasses as being in a strong or supercooled liquid state. However, the long-time trend in ϕ reverses at $\phi = 0.59$, suggesting that the driving force cannot fully overcome glassy frustration. Somewhere between 58.5% and 59% is a "sweet spot" where the energy stored in heterogenous structural relaxation is most able to relax it toward homogeneity, and is likely to drive the system to an intransient (metastable) state. This idea is reinforced by an initial increase in average coordination number for $\phi > 0.58$: the duration of the early-time growth of average coordination number increases with increasing volume fraction, which suggests that cages get more and more stiff and durable. But eventually, at least for $\phi < 0.64$, the driving force can ultimately relax the structure to a lower average coordination number, loosening particle cages. We identify this region as a "loose glass". But the degree of glassy frustration, indicated by the long-time value of normalized mean coordination number, reflects the weakening ability of the driving force to relax the structure as volume fraction increases. For very deep quenches, $\phi \geq 0.64$, the initial increase in coordination number is very slow to decay and may never relax below the initial value — giving very tight cages — and this condition worsens as the quench deepens further. This behavior suggests the emergence of an energy barrier that must be

overcome by a non-equilibrium driving force, a point we return to shortly. Overall, the long-time value of the average post-quench coordination number first goes up then goes down with increasing quench depth, giving an intuitive picture of how much free volume the system was able to access in order to relax with age. Volume relaxation provides a natural connection to thermodynamic variables, an idea we examine next.

We quantify the evolution of heterogeneous cage structure by measuring void widths between particles based on Voronoi analysis [60, 61]. The void width is defined as the shortest distance from a Voronoi edge to the nearest particle surface. The width of a void gives an idea of its size, simultaneously describing how much "wiggle room" each particle has and quantifying the distribution of thermodynamic volume. Based on geometry, the void width of three equally sized spheres when they are perfectly just in three-way contact is $d/a = 0.15$. However, the typical gap between very close neighbors will be larger than $0.15a$, because such perfect arrangement is infrequent owing to Brownian motion, a fact that is revealed by a slightly broader peak in the pair distribution function $g(r)$. We examine $g(r)$ to estimate a more realistic gap: A particle at the first trough outside the nearest-neighbor ring in $g(r)$ (which means that it is no longer coordinated with the reference particle) comes no closer than about $0.05a$ to the nearest-neighbor peak, providing guidance to select an additional average separation of $0.05a$ as the threshold for defining a coordinated pair. Thus, particles surrounding a reference particle (forming at least a triplet) are said to be coordinated with each other if their surface-to-surface distance is less than $0.05a$ (not exactly at 0), thus giving a slightly larger void width between them at around $0.20a$. This dividing line establishes a threshold between volume that is available and that which is unavailable for relaxation. The calculated distribution of free volumes is described schematically in a cartoon sketch in Figure 4 to illustrate two hypothetical liquid-like systems. The red curve represents a heterogeneous system where some colloids form clusters while others freely diffuse, leading to a bimodal distribution of void widths. The blue curve represents a more homogeneous system where colloids are evenly distributed around each other, resulting in one pronounced peak in void width distribution. We hypothesize that in colloidal glasses, right after the quench the void width distribution should be qualitatively similar to the red curve (but with a much narrower separation between the two peaks because large voids are unlikely at high volume fraction), i.e. post-quench structure is spatially heterogeneous. Subsequently, following glassy relaxation, the system should reach a void width distribution similar to the blue curve, a homogeneous system. The evolution of void space within Region 1 does not change with age, indicating that part of the structure and voids have reached metastable equilibrium. Compared to the homogeneous case, Region 2 quantifies excessive tight void space and Region 3 quantities excessive loose void space right after the quench. We envision Region 4 as an emerging intermediate-sized void space. Overall, we envision that what happens during glassy relaxation is that (tight) void space in Region 2 and (loose) void space in Region 3 are evolving toward Region 4. Such an evolution from the red curve to the blue curve, if accurate, can shed light on the mechanism driving coordination number evolution, as follows. By our definition, void widths smaller than $0.2a$ form coordinated particle pairs, thus coordination number only changes when void space evolves to grow beyond $0.2a$. In our cartoon of a liquid-like system, evolution of Region 2 towards Region 4 drives loss of coordinated

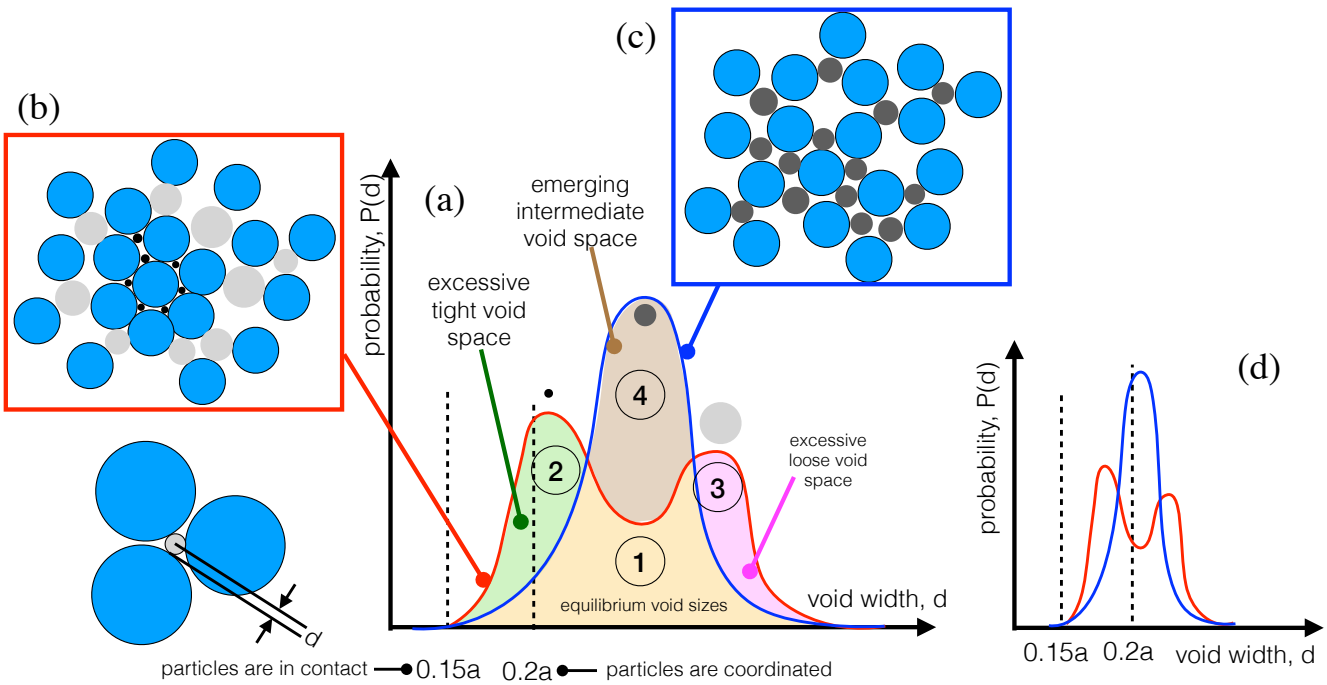

Figure 4: Examples of void width distribution. (a) A void width distribution for a liquid-like system. Red curve illustrates a heterogeneous structure with bi-modal distribution, and blue curve illustrates a homogeneous structure with only one pronounced peak. Two vertical dashed lines demonstrate two scenarios when particles are in contact and are considered coordinated, which are calculated using the triplet configuration shown in the lower left corner. (b) A possible configuration that leads to a heterogeneous void width distribution (the red curve in Panel (a)). (c) A possible configuration that shows a homogeneous distribution (the blue curve in Panel (a)). The radii of circles with different grey scales describe the representative void widths in the system, which are labeled in Panel (a) at the peaks of red and blue curves. (d) An illustration shows that in dense suspensions, the coordination threshold can intersect with Region 4, which can leads to complex coordination number evolution.

pairs, because Region 4 is entirely to the right of the threshold and Region 2 is evolving towards the right crossing the threshold. Thus, the position of $0.2a$ relative to the position of Region 4 determines the age-evolution of coordination number. For example, the coordination number can only increase (decrease) if Region 4 is entirely to the left (right) of the coordination threshold. Alternatively, one can infer that the coordination number may increase or decrease over time if Region 4 partially overlaps the coordination threshold ($0.2a$) in Figure 4(d). The distribution of void widths in the glass are likely to be very tightly grouped and can provide insight regarding our observation of Figure 3, which we analyze next.

We carried out the void width measurements as described above and in [61]. Immediately following a quench to $\phi = 0.57$ [Figure 5(a)], the distribution of void widths produces a pronounced peak near $d = 0.2a$, corresponding to an abundance of the smallest-possible voids, as well as a "shoulder" at larger void-width $d \approx 0.4a$, indicating an excess of large "defects" (volume available for relaxation) in an amorphous structure. This bimodal distribution of void widths confirms that the structure immediately after the quench is heterogeneous. As aging progresses, more intermediate-sized relaxing voids are formed, while the abundance of near-contact voids and defects shrinks. It is worth noting that the width of intermediate-sized relaxing voids is larger than the width of coordination voids at $\phi = 0.57$ (the curves fall substantially to the right of the

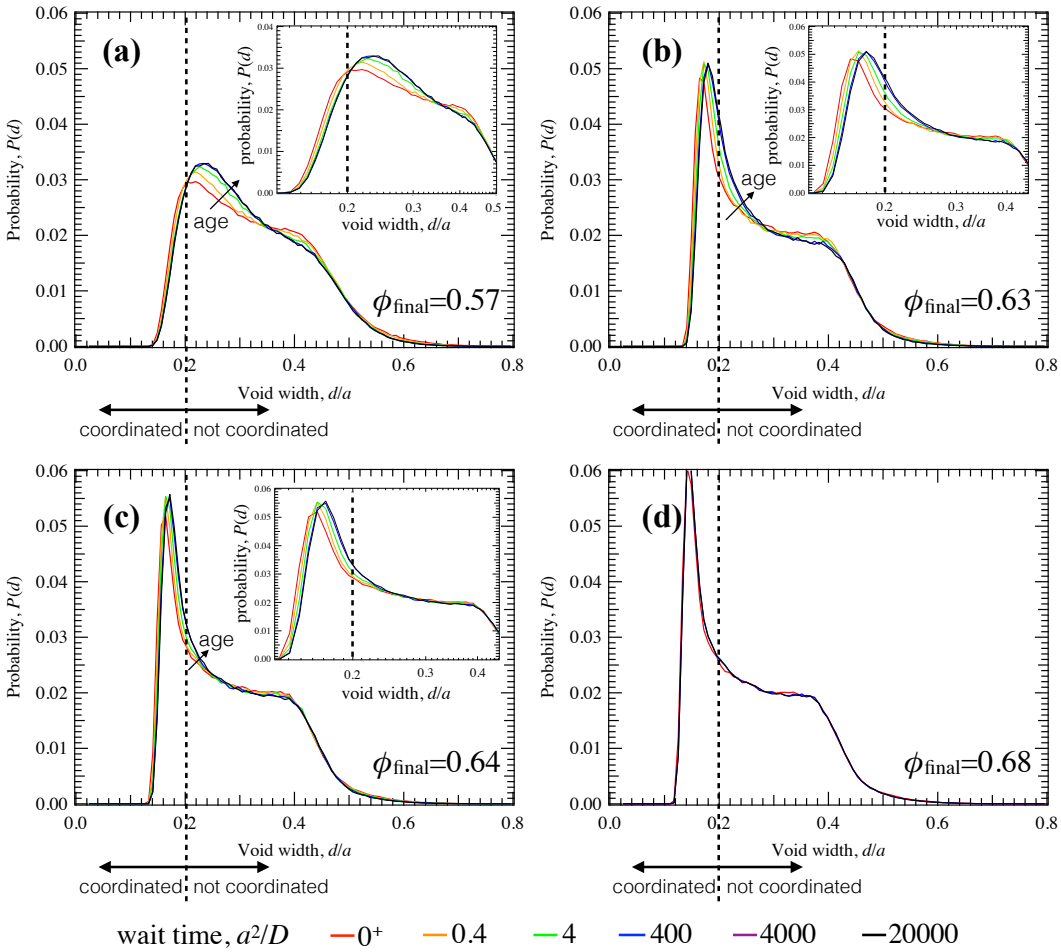

Figure 5: The void width distribution at (a) $\phi = 0.57$, (b) $\phi = 0.63$, (c) $\phi = 0.64$, and (d) $\phi = 0.68$, at different wait time as indicated in the legend. The dashed line marks the void width when particles are considered as in a coordinated pair. The insets in Panel (a-c) show the detailed evolution for the emerging intermediate-sized voids.

coordination threshold line), indicating that there is much free volume for structural relaxation, which is consistent with continuously decreasing coordination number. This transfer from tight and loose void spaces to intermediate values signals separation of coordinated pairs, although there is still persistent heterogeneity in the void width distribution in the long-time intransient state. In Figure 5(b)], we perform a deeper quench to $\phi = 0.63$, generating a tighter packing. The peak at the near-contact void space is even more pronounced and shifts to smaller values, and the separation between the peak and the "shoulder" also becomes wider, suggesting a higher level of void space heterogeneity. Notably, the first peak shifts and moves to the left of the coordination threshold; the voids represented by the region under the curve to the left of the threshold now represent rigid, smaller cages: their width is smaller than $d = 0.2a$. This decreases the amount of void volume that can relax. We recall from Figure 4 that the region subtended by the short- and long-time distribution gives the emerging intermediate void population; at $\phi = 0.63$, this area is nearly equally divided into a part to the left of the threshold and a part to the right of it, indicating that there are nearly equal numbers of rigid and loose voids in the emerging intermediate-sized void population, which explains the increase-then-decrease behavior of its average coordination

number. At $\phi = 0.64$ [Figure 5(c)], the majority of the emerging intermediate-sized voids are rigid (below the 0.2a threshold), which is again consistent with observations in Figure 3: an increase followed by a plateau of average coordination number. At very high volume fraction, $\phi = 0.68$ [Figure 5 panel (d)], the glassy relaxation is so entropically hindered that there is no free volume available, and thus structural heterogeneity of the system is completely frozen into a metastable equilibrium state. The redistribution of coordination number and void width reveals the structural relaxation as a process that smooths structural heterogeneity. Because there is no external force driving this behavior, we turn our attention to the connection of gradients in number density lead to gradients in osmotic pressure.

3.2 Osmotic pressure

For a purely repulsive colloidal suspension, osmotic pressure measures the normal stress the particles exert on a fictitious wall enclosing them, as illustrated in the sketch in Figure 6. The osmotic pressure is thus connected to the concentration gradient in the system and describes the tendency for the particle phase to diffusively expand and sample an ever-larger space. For the example in Figure 4(b), the cluster creates a higher concentration relative to its surroundings; Brownian motion will act to make uniform their distribution. Equivalently stated, the particle phase will expand to reduce the free energy by maximizing entropy. The particles will thus push outward on the walls of a surrounding fictitious container at the location of the dashed circle, exerting a positive osmotic pressure. In an equilibrium suspension, there is a balance between the normal stresses of particles inside the fictitious container pushing outward and of particles outside the container pushing inward, indicating that the local concentration is the same throughout the suspension. However, for a non-equilibrium suspension such as the one shown in Figure 4(b) or Figure 6, there is a stronger normal stress for particles pushing outward than particles pushing inward, due to non-uniform local concentrations which in turn generates a higher osmotic pressure than the equilibrium value. This non-equilibrium osmotic pressure provides a driving force for particles to rearrange until they find their equilibrium positions, during which osmotic pressure decreases as local number density becomes homogeneous. This process reveals a gradient in the free energy landscape between initial and final state; decreasing osmotic pressure thus can be viewed as driving a minimization process of free energy, by recalling that there is a natural mechanical / thermodynamic connection between the osmotic pressure and the free energy, as follows. The particle-phase stress in a freely-draining suspension is given by $\boldsymbol{\Sigma}^P = -nkT\boldsymbol{I} + \langle \boldsymbol{r}\boldsymbol{F}^P \rangle$, where the interparticle force for hard spheres is the gradient of the interparticle potential, $\boldsymbol{F}^P = \boldsymbol{F}^{HS} = -\nabla V(r)$. The potential energy of the system is thus related directly to the osmotic pressure, $\Pi^P = -\boldsymbol{I} : \langle \boldsymbol{\Sigma}^P \rangle / 3$. Because colloidal glasses are a non-equilibrium material characterized by evolving heterogeneity of structure, we expect osmotic pressure to exhibit different values immediately post-quench versus at long times post-quench. We hypothesized that this difference in osmotic pressure is a driving force that acts to minimize free energy along the energy landscape, relaxing the glass toward the metastable state.

We measured the particle-phase osmotic pressure immediately following quenches to a range

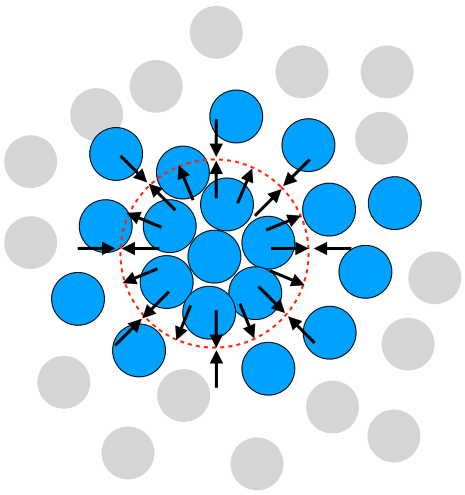

Figure 6: An illustration of imbalanced osmotic pressure in a non-equilibrium suspension.

of volume fractions and monitored its evolution throughout simulation. Because we have asked whether osmotic pressure drives a spontaneous relaxation process, we compare the long-time value of the pressure to previously-established metastable equilibrium osmotic pressure for hard-sphere colloidal systems. The data are plotted together in Figure 8. Four sets of data from previous studies are shown, which do not *quench* into the glass but rather enforce a particle configuration consistent with the (at least locally) minimized energy state at a given volume fraction. The Carnahan-Starling equation of state [62] predicts an osmotic pressure based on extrapolation of the equilibrium liquid line into the supercooled region, valid for quenches up to just below 50% volume fraction. Speedy [31] and later, Rintoul and Torquato [63] employed an event-driven simulation technique to generate an initial configuration for a monodisperse suspension of colloidal hard spheres, spanning the liquid to the glass region, up to $\phi = 0.62$. Speedy used a fixed number of collision events to seek equilibration for all volume fractions; meanwhile Rintoul and Torquato followed their event-driven construction by allowing the configuration to evolve via Brownian motion. Crystallization occurred almost immediately in both studies for $0.54 \leq \phi \leq 0.62$, confirming the tenuous metastability of the original configuration for monodisperse hard spheres. Both studies *extrapolated* the osmotic pressure to reach $\phi = 0.64$, enforcing rather than predicting divergence by imposing a generic power-law fit (another factor undermining the equilibrium assumption). Because these methods model monodisperse systems, the three sets of data are able to establish a baseline metastable state, but the fact that the systems crystallize immediately reinforces the idea we discussed in the Introduction that the metastable state is quite difficult to maintain. Meanwhile, in our simulations with polydisperse hard spheres, we find that immediately following the quench, the osmotic pressure is higher than the metastable state, and it remains so for long times, without crystallization (cf §2), i.e., to approach the metastable state, we must age the system over long times. Recalling the discussion in the Introduction, this supports the view that the metastable line is very difficult to achieve directly: for monodisperse systems, one must artificially construct *in silico* a configuration consistent with the locally lowest energy, but any subsequent Brownian motion kicks the system off that line onto the crystal line. For polydisperse

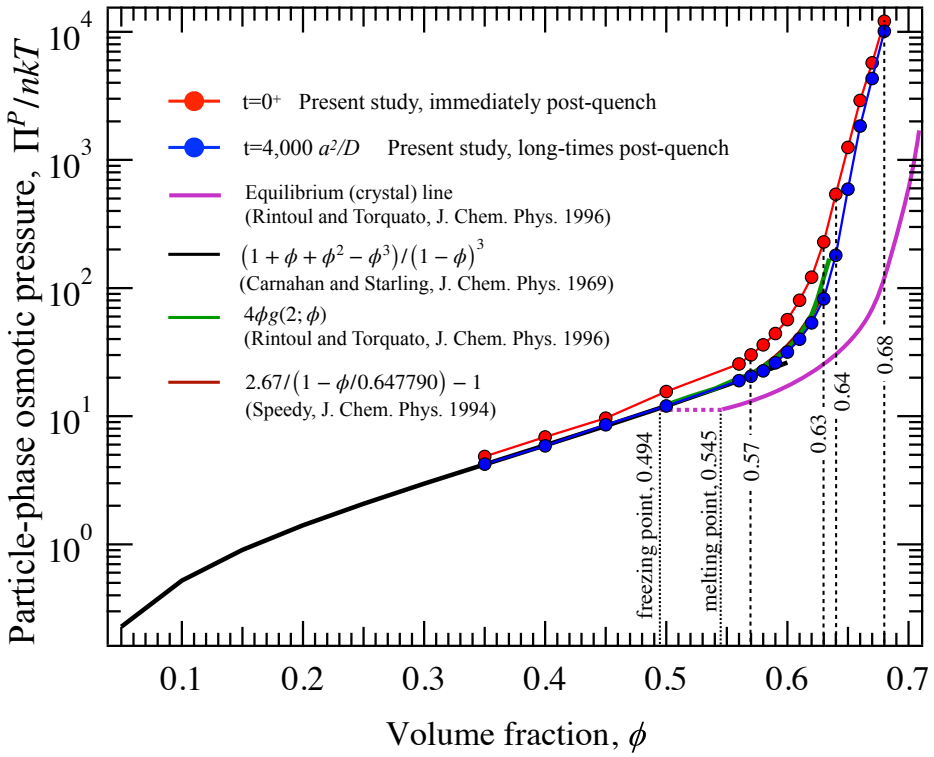

Figure 7: Pair contribution of osmotic pressure as a function of volume fraction, compared with values from literature. Two sets of data from the present study are shown: red circles are osmotic pressure just after the jump, and blue circles are osmotic pressure measured at $4,000a^2/D$.

spheres, the system gets kicked "upwards" off the equilibrium line to a non-equilibrium state, and must relax kinetically to reach the metastable state, where it remains for very long times. Overall, the osmotic pressure in our polydisperse system evolved spontaneously — but slowly — toward a metastable state. We believe the spontaneous process, reduction of energy, occurs via structural relaxation as discussed above, and is driven by non-equilibrium osmotic pressure. The difference between the initial and final osmotic pressure represents a gradient in the free energy between the initially more heterogeneous structure and the long-time more homogeneous one, setting an energy barrier that particles must overcome to reach metastable equilibrium via diffusion, which should provide a driving force for glassy relaxation.

We connect the age-relaxation of osmotic pressure in Figure 7 with the relaxation of coordination number and void widths by examining the osmotic pressure plot at the selected values of the quench in Figures 5(a-d). Recall that the average coordination number eventually decreases for any quench to $\phi < 0.64$, as the system accesses and homogenizes free volume — indicating the action of a robust driving force toward relaxation. But for $\phi \geq 0.64$, the average coordination number increases post-quench and cannot subsequently relax (Figure 3). The origin of this frustration is very limited accessible free volume, and when the system accesses it, the relaxation brings particles further into contact (Figure 5). The increase in coordination number occurs at short times post-quench, corresponding to the $t = 0^+$ (red) pressure curve in Figure 7; there is a correspondence between whether the coordination number eventually decreases and how far the long-time "excess" osmotic pressure (blue curve) is from the metastable pressure. This suggests a

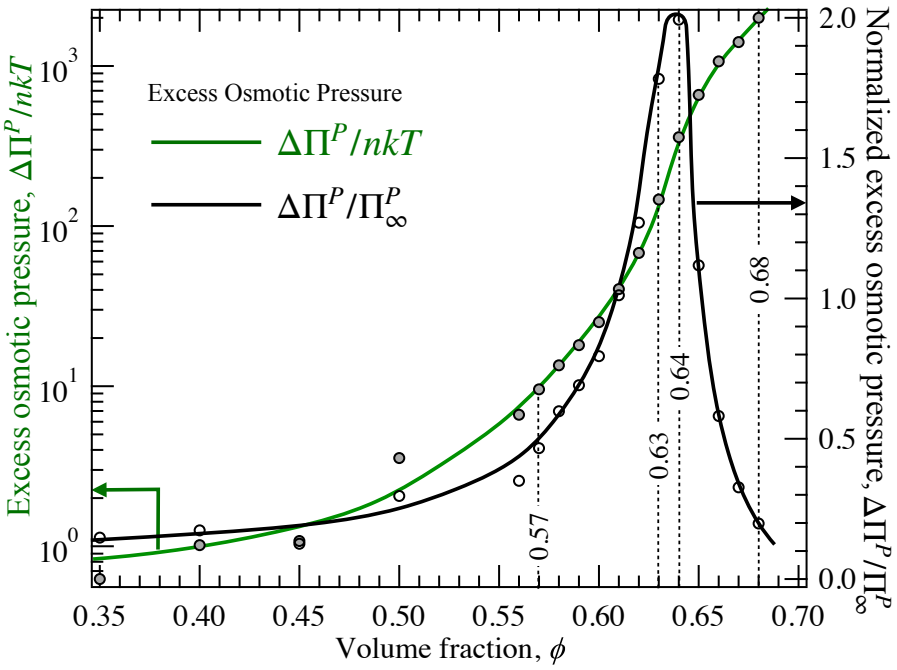

Figure 8: Absolute and normalized osmotic pressure overshoot as a function of volume fraction, plotted on the left and right vertical axes, respectively. The solid lines are guide to the eye.

closer look at the excess osmotic pressure.

In Figure 8, we examine the the excess osmotic pressure: the non-equilibrium contribution to the osmotic pressure, which is the difference between its initial post-quench (non-equilibrium) value $\Pi^P(t=0^+)$ and its long-time metastable value, Π^P_∞. Figure 7 suggested that this difference, $\Delta\Pi^P \equiv \Pi^P(t=0^+) - \Pi^P_\infty$, sets the driving force for glassy relaxation of heterogeneous structure. To interrogate this idea, we examine the magnitude of the excess osmotic pressure $\Delta\Pi^P$ (green curve). Throughout the liquid region at low volume fractions, $\Delta\Pi^P$ is $O(1)$, indicating that the system has plenty of room to relax. The excess pressure grows dramatically at $\phi \geq 0.55$, suggesting a strong driving force for relaxation with increasing volume fraction. At quenches in the putative glassy region, $\Delta\Pi^P$ continues to grow, driving structural relaxation toward the metastable intransient state. However, there is an inflection point at $\phi = 0.63$. To take a closer look, we normalize the excess osmotic pressure by the metastable pressure, $\Delta\Pi^P/\Pi^P_\infty$. Mechanistically, the metastable osmotic pressure Π^P_∞ becomes very high as particle diffusion becomes very slow, setting a characteristic pressure scale for relaxation, where comparatively larger excess pressure can drive relaxation and comparatively weaker excess pressure cannot. This normalized excess pressure $\Delta\Pi^P/\Pi^P_\infty$ increases from very small values in the liquid state to a peak just following the inflection point, at around $\phi = 0.64$.

We infer that, during the rapid growth regime $0.55 \leq \phi < 0.64$, the non-equilibrium osmotic pressure accumulated during the quench is a strong driving force, strong enough to overcome steric hindrance and drive relaxation. It reaches a peak that roughly coincides with the phase boundary between the loose and the tight glass we identified in Figure 3 from average coordination number

measurements. When the peak at $\phi \approx 0.64$ is passed, the normalized excess pressure $\Delta\Pi^P/\Pi^P_\infty$ drops precipitously — it is strong enough to drive particles into a more jammed condition consistent with a very high metastable pressure, where relaxation dynamics are extremely hindered and slow, essentially freezing the structure.

Overall, the excess osmotic pressure drives spontaneously structural homogenization that either relaxes the system to an intransient metastable state where particle dynamics persist, or it vitrifies the system energetically close to but kinetically far from the metastable state. We pause to make a connection to the free energy of the system. As noted in §2, the osmotic pressure in a hard-sphere system derives directly from the potential energy. This potential energy evolves (decreases) alongside the system entropy, which increases during structural homogenization. Evidently the osmotic pressure acts to minimize the free energy as a glassy system ages, acting as a driving force in a spontaneous transition from liquid to glass.

4 Conclusions

Efforts to explain the colloidal glass transition via equilibrium thermodynamic theories are undermined by the fact that vitrification by definition drives the system off the equilibrium phase boundary. Metastable equilibrium approaches offer an alternative, but the liquid-state models for particle dynamics central to such theories lead directly to well-known shortcomings of the predicted glass transition. At the heart of this challenge is the implicit assumption typically invoked in the literature that colloidal glasses form within the metastable state, which effectively bypasses the search for a driving force for vitrification and glassy aging, and indeed its connection with a long-time metastable state. We suspect that the metastable state is itself an underlying or fictitious state: either a system will immediately fall off the metastable line to the crystalline state or get pushed off the metastable line to the non-equilibrium glassy 'state'. The fact that colloidal glasses age is central to making progress with a model for vitrification; to wit, it is widely accepted in the experimental literature that *molecular* glass-formers get driven off the metastable liquid line and must "age to equilibrium". Thus, a central aspect to computational modeling of colloidal vitrification is quenching into the glass in the presence of Brownian motion and particle interactions — rather than artificially constructing an amorphous dense solid consistent with a glass.

To model the interplay between quench rate and particle dynamics, we constructed a computational model of a large system of polydisperse hard-sphere colloids and executed a series of independent volume-fraction jumps to various depths in the glassy region. By investigating structure via a new approach — monitoring coordination number — we discovered that post-quench structural relaxation changes average coordination number. Following a quench to $\phi \geq 0.56$, relaxation results in one of three final states: a supercooled liquid for $0.56 \leq \phi \leq 0.58$ where the average coordination number decreases continuously over time; a "loose" glass for $0.58 \leq \phi < 0.64$, where average coordination number first increases then decreases below the initial quenched value over time; or a "tight" glass for $\phi \geq 0.64$, where coordination number increases and then plateaus

with age. Thus, a loose glass has the potential for relaxing spontaneously toward a lower-energy metastable state (possibly even crystallizing) but a tight glass is permanently frozen in a non-equilibrium state. This suggests the existence of a driving force for structural relaxation that can either drive the system to a more relaxed, less frustrated state or toward a more condensed, rigid (vitrified) state.

The evolution of coordination number gave us an intuitive picture that there was heterogeneous distribution of the free volume that the system was able to access in order to relax with age. We thus leveraged a new method [61] to monitor the distribution of void spaces in a glass, giving a sensitive measure of structural heterogeneity. Moreover, volume relaxation is connected to thermodynamic variables, making its study our natural next step.

The initial distribution of void spaces throughout the glass revealed that the quench induces not just denser structure but also heterogeneous structure. We discovered that void density is transferred away from near-contact and from large-void values, forming intermediate-sized voids, a process that smooths the distribution of volume. We interpret the size of intermediate-sized relaxing voids relative to those of the coordination threshold as a measure of accessible free volume, which dictates the evolution of coordination number. We identified three scenarios for the post-quench evolution of void widths that match the three regimes identified by the average coordination-number evolution. For quenches at and below $\phi = 0.57$, there is substantial post-quench accessible volume that allows the system to continuously reduce its mean coordination number. Deep into the glass, $\phi = 0.63$, a substantial portion of the free volume is *in*accessible, but after a slight barrier, the glass pushes through to access it. Very deep into the glass, $\phi = 0.64$, there is hardly any accessible free volume except that which brings any minimally mobile particles into contact and freezes them. The combined evaluation of coordination number and accessible free volume revealed a dividing line between quenches that can reach a metastable state and quenches so deep that they remain permanently out of equilibrium.

Finally, we leveraged the natural connection between diffusion and osmotic pressure to identify a connection between vitrification, structural relaxation, and a driving force for a spontaneous process. We found that the osmotic pressure in colloidal glasses evolves from an initially high value immediately post-quench to an intransient value at long times that defines a metastable equilibrium state. We find two competing actions of the osmotic pressure that set the behavior of structural relaxation. The excess osmotic pressure induced by the quench provides a driving force for glassy relaxation, but the metastable equilibrium osmotic pressure tends to hinder particle dynamics for relaxation. At $\phi < 0.64$, the excess osmotic pressure is much larger than the metastable equilibrium pressure, setting a robust driving force for relaxation where particles can eventually overcome the barrier to relax to a state that is less compact — thus particles can explore states with lower free energy. However, this driving force weakens at $\phi \geq 0.64$, whereupon it cannot drive particles pass the energy barrier formed by tight cages, leaving the system frozen into a tight configuration indefinitely.

Overall, we found that number-density gradients and osmotic pressure accumulate during a colloidal liquid-to-solid quench, and the excess pressure subsequently drives diffusive relaxation of the heterogeneous structure. This process is necessary for a glass to reach the metastable state

— the system cannot traverse the liquid line from the equilibrium region to follow directly along the supercooled metastable line; rather, vitrification requires departure from and return to the metastable line, due to energy storage via persistent non-equilibrium structure, and energy release via age relaxation, respectively. We identify glassy arrest as taking place after the quench, as the structure attempts to relax local density gradients. We have shown that non-equilibrium osmotic pressure drives this relaxation and, paradoxically, this relaxation causes arrest by driving particles into higher-coordination number configurations. The volume fraction where there is a strictly non-decreasing average coordination number following the quench, associated with an abrupt transition in the osmotic pressure, determines a well-defined ϕ_g for hard-sphere colloids; for our system with 7% polydispersity, $0.63 < \phi_g \leq 0.64$. We argued that, because the osmotic pressure in a hard-sphere system derives directly from the potential energy, which decreases alongside the increasing system entropy during structural homogenization, evidently the osmotic pressure acts to minimize the free energy as a glassy system ages, acting as a driving force in a spontaneous transition from liquid to glass.

Acknowledgements

The authors thank G. B. McKenna, E. R. Weeks, M. Fuchs, and E. Del Gado for many helpful conversations. The authors wish to thank B. K. Ryu for help with the void width calculations. The authors also acknowledge support from the National Science Foundation Grant No. CBET-1506079, an Office of Naval Research Director of Research Early Career Grant No. N000141812105, and the computational resources from the National Science Foundation Extreme Science and Engineering Discovery Environment (XSEDE) Research Award No. OCI-1053575 utilizing TACC and Stampede.

References

[1] J Buitink. *Biological glasses : nature's way to preserve life*. PhD thesis, 88, Laboratorium voor Biofysica,, 2000.

[2] Joanna Aizenberg, Vikram C. Sundar, Andrew D. Yablon, James C. Weaver, and Gang Chen. Biological glass fibers: Correlation between optical and structural properties. *Proceedings of the National Academy of Sciences*, 101(10):3358–3363, 2004.

[3] C. Jaco Klok. Biological glass: A strategy to survive desiccation and heat. *Journal of Experimental Biology*, 213(7):iv–iv, 2010.

[4] Bradley R. Parry, Ivan V. Surovtsev, Matthew T. Cabeen, Corey S. OHern, Eric R. Dufresne, and Christine Jacobs-Wagner. The bacterial cytoplasm has glass-like properties and is fluidized by metabolic activity. *Cell*, 156(1):183 – 194, 2014.

[5] Michel Aegerter and Martin Mennig. *Sol-Gel Technologies for Glass Producers and Users*. 01 2004.

[6] Gary L Hunter and Eric R Weeks. The physics of the colloidal glass transition. *Rep. Prog. Phys.*, 75(6):066501, 2012.

[7] Peter J. Lu and David A. Weitz. Colloidal particles: Crystals, glasses, and gels. *Annu. Rev. Condens. Matter Phys.*, 4(1):217–233, 2013.

[8] Louise Slade, Harry Levine, James Ievolella, and Martha Wang. The glassy state phenomenon in applications for the food industry: Application of the food polymer science approach to structurefunction relationships of sucrose in cookie and cracker systems. *Journal of the Science of Food and Agriculture*, 63(2):133–176, 1993.

[9] Yrjö H. Roos. Glass transition temperature and its relevance in food processing. *Annual Review of Food Science and Technology*, 1(1):469–496, 2010. PMID: 22129345.

[10] W. van Megen and I. Shook. Equilibrium properties of suspensions. *Adv. Colloid Interface Sci.*, 21(1):119 – 194, 1984.

[11] Daan Frenkel. Order through disorder: entropy strikes back. *Physics World*, 6(2):24–25, feb 1993.

[12] Paul Bartlett. Fractionated crystallization in a polydisperse mixture of hard spheres. *The Journal of Chemical Physics*, 109(24):10970–10975, 1998.

[13] Paul Bartlett and Patrick B. Warren. Reentrant melting in polydispersed hard spheres. *Phys. Rev. Lett.*, 82:1979–1982, Mar 1999.

[14] Moreno Fasolo and Peter Sollich. Equilibrium phase behavior of polydisperse hard spheres. *Phys. Rev. Lett.*, 91:068301, Aug 2003.

[15] W Götze and L Sjögren. Relaxation processes in supercooled liquids. *Rep. Prog. Phys*, 55(3):241, 1992.

[16] Adolfo J. Banchio, Gerhard Ngele, and Johan Bergenholtz. Viscoelasticity and generalized stokeseinstein relations of colloidal dispersions. *J. Chem. Phys.*, 111(18):8721–8740, 1999.

[17] T. R. Kirkpatrick, D. Thirumalai, and P. G. Wolynes. Scaling concepts for the dynamics of viscous liquids near an ideal glassy state. *Phys. Rev. A*, 40:1045–1054, Jul 1989.

[18] Vassiliy Lubchenko and Peter G. Wolynes. Theory of structural glasses and supercooled liquids. *Annu. Rev. Phys. Chem.*, 58(1):235–266, 2007.

[19] T. R. Kirkpatrick and D. Thirumalai. Colloquium: Random first order transition theory concepts in biology and physics. *Rev. Mod. Phys.*, 87:183–209, Mar 2015.

[20] Kenneth S. Schweizer and Erica J. Saltzman. Entropic barriers, activated hopping, and the glass transition in colloidal suspensions. *The Journal of Chemical Physics*, 119(2):1181–1196, 2003.

[21] Kenneth S. Schweizer. Derivation of a microscopic theory of barriers and activated hopping transport in glassy liquids and suspensions. *The Journal of Chemical Physics*, 123(24):244501, 2005.

[22] Stephen Mirigian and Kenneth S. Schweizer. Elastically cooperative activated barrier hopping theory of relaxation in viscous fluids. i. general formulation and application to hard sphere fluids. *The Journal of Chemical Physics*, 140(19):194506, 2014.

[23] Stephen Mirigian and Kenneth S. Schweizer. Elastically cooperative activated barrier hopping theory of relaxation in viscous fluids. ii. thermal liquids. *The Journal of Chemical Physics*, 140(19):194507, 2014.

[24] J. Galen Wang, Qi Li, Xiaoguang Peng, Gregory B. McKenna, and Roseanna N. Zia. "dense diffusion" in colloidal glasses: short-ranged long-time self-diffusion as a mechanistic model for relaxation dynamics. *Soft Matter*, accepted, 2020.

[25] P. N. Pusey and W. van Megen. Observation of a glass transition in suspensions of spherical colloidal particles. *Phys. Rev. Lett.*, 59:2083–2086, Nov 1987.

[26] W. van Megen and S. M. Underwood. Glass transition in colloidal hard spheres: Measurement and mode-coupling-theory analysis of the coherent intermediate scattering function. *Phys. Rev. E*, 49(5):4206–4220, 1994.

[27] A. J. Kovacs. Transition vitreuse dans les polym'eres amorphes. etude ph'enomenologique. In *Fortschritte Der Hochpolymeren-Forschung*, chapter 3. Springer, Berlin Heidelberg, 1964.

[28] G. B. McKenna. Physical aging in glasses and composites. In Kishore V. Pochiraju, Gyaneshwar P. Tandon, and Gregory A. Schoeppner, editors, *Long-Term Durability of Polymeric Matrix Composites*, chapter 7. Springer, New York, 2012.

[29] Pedro Ramírez-González and Magdaleno Medina-Noyola. General nonequilibrium theory of colloid dynamics. *Phys. Rev. E*, 82:061503, Dec 2010.

[30] P. Mendoza-Méndez, E. Lázaro-Lázaro, L. E. Sánchez-Díaz, P. E. Ramírez-González, G. Pérez-Ángel, and M. Medina-Noyola. Crossover from equilibration to aging: Nonequilibrium theory versus simulations. *Phys. Rev. E*, 96:022608, Aug 2017.

[31] Robin J. Speedy. On the reproducibility of glasses. *J. Chem. Phys.*, 100(9):6684–6691, 1994.

[32] Alfons van Blaaderen and Pierre Wiltzius. Real-space structure of colloidal hard-sphere glasses. *Science*, 270(5239):1177–1179, 1995.

[33] Katharina Vollmayr, Walter Kob, and Kurt Binder. Cooling-rate effects in amorphous silica: A computer-simulation study. *Phys. Rev. B*, 54:15808–15827, Dec 1996.

[34] A. Einstein. Zur theorie der brownschen bewegung. *Annalen der Physik*, 324(2):371–381, 1906.

[35] G. K. Batchelor. The effect of brownian motion on the bulk stress in a suspension of spherical particles. *Journal of Fluid Mechanics*, 83(1):97117, 1977.

[36] W.B. Russel. The huggins coefficient as a means for characterizing suspended particles. *Journal of the Chemical Society, Faraday Transactions 2: Molecular and Chemical Physics*, 80(1):31–41, 1984.

[37] Jeffrey F. Morris and John F. Brady. Self-diffusion in sheared suspensions. *Journal of Fluid Mechanics*, 312:223252, 1996.

[38] R. N. Zia and J. F. Brady. Microviscosity, microdiffusivity, and normal stresses in colloidal dispersions. *Journal of Rheology*, 56(5):1175–1208, 2012.

[39] Henry C. W. Chu and Roseanna N. Zia. Active microrheology of hydrodynamically interacting colloids: Normal stresses and entropic energy density. *Journal of Rheology*, 60(4):755–781, 2016.

[40] Roseanna N. Zia, Benjamin J. Landrum, and William B. Russel. A micro-mechanical study of coarsening and rheology of colloidal gels: Cage building, cage hopping, and smoluchowski's ratchet. *J. Rheol.*, 58(5):1121–1157, 2014.

[41] Steve Plimpton. Fast parallel algorithms for short-range molecular dynamics. *J. Comput. Phys.*, 117(1):1 – 19, 1995.

[42] S.I. Henderson, T.C. Mortensen, S.M. Underwood, and W. van Megen. Effect of particle size distribution on crystallisation and the glass transition of hard sphere colloids. *Physica A: Statistical Mechanics and its Applications*, 233(1):102 – 116, 1996.

[43] P. N. Pusey, E. Zaccarelli, C. Valeriani, E. Sanz, Wilson C. K. Poon, and Michael E. Cates. Hard spheres: crystallization and glass formation. *Philosophical Transactions of the Royal Society A: Mathematical, Physical and Engineering Sciences*, 367(1909):4993–5011, 2009.

[44] Paul J. Steinhardt, David R. Nelson, and Marco Ronchetti. Bond-orientational order in liquids and glasses. *Phys. Rev. B*, 28:784–805, Jul 1983.

[45] J. BERGENHOLTZ, J. F. BRADY, and M. VICIC. The non-newtonian rheology of dilute colloidal suspensions. *J. Fluid Mech.*, 456:239275, 2002.

[46] ADITYA S. KHAIR and JOHN F. BRADY. Single particle motion in colloidal dispersions: a simple model for active and nonlinear microrheology. *J. Fluid Mech.*, 557:73117, 2006.

[47] Aditya S. Khair, Manuj Swaroop, and John F. Brady. A new resistance function for two rigid spheres in a uniform compressible low-reynolds-number flow. *Phys. Fluids*, 18(4):043102, 2006.

[48] Manuj Swaroop and John F. Brady. The bulk viscosity of suspensions. *J. Rheol.*, 51(3):409–428, 2007.

[49] Axel Brünger, Charles L. Brooks, and Martin Karplus. Stochastic boundary conditions for molecular dynamics simulations of st2 water. *Chem. Phys. Lett.*, 105(5):495 – 500, 1984.

[50] M. P. Allen and D. J. Tildesley. *Computer Simulation of Liquids*. Oxford: Clarendon Press, 1987.

[51] D. M. Heyes and J. R. Melrose. Brownian dynamics simulations of model hard-sphere suspensions. *J. Non-Newtonian Fluid Mech.*, 46(1):1–28, 1993.

[52] William G. Hoover and Francis H. Ree. Melting transition and communal entropy for hard spheres. *The Journal of Chemical Physics*, 49(8):3609–3617, 1968.

[53] W. Schaertl and H. Sillescu. Brownian dynamics of polydisperse colloidal hard spheres: Equilibrium structures and random close packings. *Journal of Statistical Physics*, 77(5):1007–1025, Dec 1994.

[54] Johan Mattsson, Hans M. Wyss, Alberto Fernandez-Nieves, Kunimasa Miyazaki, Zhibing Hu, David R. Reichman, and David A. Weitz. Soft colloids make strong glasses. *Nature*, 462(7269):83–86, 2009.

[55] Roger Bonnecaze and Michel Cloitre. *Micromechanics of Soft Particle Glasses*, volume 236, pages 117–161. 07 2010.

[56] Xiaojun Di, K. Z. Win, Gregory B. McKenna, Tetsuharu Narita, François Lequeux, Srinivasa Rao Pullela, and Zhengdong Cheng. Signatures of structural recovery in colloidal glasses. *Phys. Rev. Lett.*, 106:095701, Feb 2011.

[57] Yu Ho Wen, Jennifer L. Schaefer, and Lynden A. Archer. Dynamics and rheology of soft colloidal glasses. *ACS Macro Letters*, 4(1):119–123, 2015.

[58] Adrian-Marie Philippe, Domenico Truzzolillo, Julian Galvan-Myoshi, Philippe Dieudonné-George, Véronique Trappe, Ludovic Berthier, and Luca Cipelletti. Glass transition of soft colloids. *Phys. Rev. E*, 97:040601, Apr 2018.

[59] Lilian C. Johnson and Roseanna N. Zia. Phase mechanics of colloidal gels: osmotic pressure drives non-equilibrium phase separation. *Soft Matter*, pages –, 2021.

[60] Georges Voronoi. Nouvelles applications des paramtres continus la thorie des formes quadratiques. premier mmoire. sur quelques proprits des formes quadratiques positives parfaites. *Journal fr die reine und angewandte Mathematik*, 133:97–178, 1908.

[61] Brian K. Ryu and Roseanna N. Zia. Method for characterizing microscopic void structure in porous media. *to be submitted*, 2020.

[62] Norman F. Carnahan and Kenneth E. Starling. Equation of state for nonattracting rigid spheres. *J. Chem. Phys.*, 51(2):635–636, 1969.

[63] M. D. Rintoul and S. Torquato. Computer simulations of dense hardsphere systems. *J. Chem. Phys.*, 105(20):9258–9265, 1996.